Chapter 23
Effect of Shock Normal Orientation Fluctuations on Field-Aligned Beam Distributions

K. Meziane, A.M. Hamza, M. Wilber, M.A. Lee, C. Mazelle, E.A. Lucek, T. Hada, and A. Markowitch

Abstract We address the unsolved question of how foreshock field-aligned beam (FAB) parallel temperatures are produced. Studies including numerical simulations and recent observations have indicated that shocks can be nonstationary and include embedded spatial structures with varied scales. As a first step towards assessing the impact of such variability on backstreaming ions, we examine how a randomly distributed shock normal direction will affect FAB parallel velocity ($v_{\parallel}$) distributions. Assuming that the FABs are produced in a quasi-adiabatic reflection process at the shock, we derive a probability distribution function for $v_{\parallel}$. These derived distributions exhibit second, third and fourth order moments that agree well with the observations for a large range of reflection efficiencies δ, and depend strongly upon the average angle between the magnetic field and the shock normal θ_{Bn0}. Best agreement is obtained for fluctuations of the normal orientation of a few degrees about a nominal direction. The derived model predicts a strong correlation between the shock geometry (θ_{Bn0}) and the moments of the parallel velocity distribution, but with stronger tails extending to higher values of θ_{Bn0}, a trend opposite to the observations.

K. Meziane (✉) and A.M. Hamza
Physics Department, University of New Brunswick, Canada
e-mail: karim@unb.ca

M. Wilber
Space Sciences Laboratory, University of California, Berkeley, USA

M.A. Lee
Space Science Center, University of New Hampshire, Durham, USA

C. Mazelle
Centre d'Etudes Spatiales des Rayonnements, Toulouse, France

E.A. Lucek
Space and Atmospheric Physics, The Blackett Laboratory, Imperial College, London, UK

T. Hada
ESST, Kyushu University, Fukuora, Japan

A. Markowitch
Laboratoire de Physique et Astroparticules, Université de Montpellier, France

H. Laakso et al. (eds.), *The Cluster Active Archive*, Astrophysics and Space Science Proceedings, DOI 10.1007/978-90-481-3499-1_23,

23.1 Introduction

It is now established that ion beams roughly propagating sunward along the interplanetary field lines are ubiquitous upstream of the Earth's quasi-perpendicular bow shock [7, 21, and references therein]. These field-aligned beams (FABs) are found on interplanetary magnetic field (IMF) lines connecting to the shock with angles to the shock normal θ_{Bn} ranging from 40° to 70° [2]. The basic properties of FABs including density and speed are very well known, with both density and speed controlled by the shock geometry. Tenuous and high-speed beams are likely to originate at a location on the shock at which the geometry is quasi-perpendicular while denser, slower beams emerge from oblique configurations. Geometric arguments indicate, and observations confirm, that the beam speeds should be 1–2 × the shock speed

$$V_s = -v_{sw}\frac{\cos\theta_{Vn}}{\cos\theta_{Bn}}, \tag{23.1}$$

where θ_{Vn} is the angle between the local shock normal and the direction of the flow, and v_{sw} is flow (or the solar wind) speed; V_s is the speed at which the shock moves parallel to the magnetic field in the solar wind frame. Beam densities vary considerably, from <0.1% to a few % of the incident solar wind density.

An exhaustive investigation of FAB thermal energy has been carried out only recently [14]. In a prior study, [13] showed that the reduced FAB distributions are organized into two categories: those with nearly-Maxwellian profiles, and those exhibiting enhanced high energy tails.

In [14], when considering only nearly-Maxwellian distributions, found that FAB parallel thermal energy is dependent upon the solar wind speed and weakly sensitive to the shock geometry. They showed that the parallel thermal speed normalized to the solar wind speed, $\sigma_\parallel$, obtained from fitting the core distribution to a Maxwellian form, is in the range 0.27–0.33. The inclusion of the high energy tail, when present, will likely lead to a measured standard deviation Σ that is higher than $\sigma_\parallel$.

Despite a precise knowledge of FAB characteristics, a comprehensive model that accounts for the production mechanism is still a topic of active research. Relatively recent investigations based upon Cluster observations found FABs with significant densities for quasi-perpendicular shock geometries [9]. Simple specular reflection should return ions to the shock in these geometries, but measurements in the foot of the shock show phase space densities in the escape cone sufficient for producing the FABs [15], while distributions downstream lack these [9]. One possibility is that these ions have been pitch-angle scattered into the escape cone following the specular reflection [9]; these latter populations are always produced by supercritical shocks. All the suggested mechanisms are geometry dependent; however, it is still not clear, when discrepancies between observations and models exist, whether they are due to uncertainties in determinations of the geometry or are inherent to theoretical models. It is not the purpose of this study to test the different FAB production mechanisms; we only consider a simple, quasi-adiabatic reflection process. A similar approach could be applied for other mechanisms. The reflection

mechanism assumes that a fraction of the incoming solar wind ions reflects off the shock in a manner that approximately conserves energy and the first adiabatic invariant $\mu = v_\perp^2/B$. Based on this assumption, [20] derived the energy gain in the shock frame. As previously mentioned, the model falls short of accounting for FAB thermalization or reflection efficiency, although bulk speed predictions are satisfactory [17]. As with all simple analytical models, the shock surface is treated as planar over scales of an ion gyroradius.

This letter is the first attempt to account for the FAB parallel thermal energy using a geometric particle reflection model (Perpendicular temperatures for FABs may be determined by unrelated considerations, and are not addressed here). Here we employ quasi-adiabatic, instantaneous reflection at a shock having a local normal that exhibits small, normally-distributed fluctuations in orientation from an average. This model has been motivated by recent studies, including observations and simulations, of shock non-stationarity [8, 10, 11, 18] as well as the presence of spatial irregularities on the shock surface [16]. In the next section, we present and briefly discuss typical velocity distribution functions of FABs observed by the Cluster/CIS experiment. The impact of the velocity filtering on the distributions is briefly considered in Section 23.3. In Section 23.4, we describe the model, and in Section 23.5 present the results. Finally, we discuss these results and compare them with observations in Section 23.6.

23.2 Foreshock FAB Reduced Parallel Distribution Functions

Figure 23.1 displays a sample of reduced parallel distribution functions associated with FABs observed upstream of Earth's bow shock. The dashed red lines correspond to the best fit using a shifted Maxwellian with a standard deviation $\sigma_\parallel$. The figure illustrates typical FAB distributions present in the terrestrial foreshock. These often exhibit high energy tails with varying degrees of hardness. We note that there appear to be inflection points in some of the tails, such as in the distributions (d), (g) and (j). Preliminary studies suggest that beams in more perpendicular geometries have nearly Maxwellian distribution profiles [13]. The distributions of Fig. 23.1 are observed at various distances from the shock as indicated by the values of D (in R_E) inside each panel. It is important to notice that the distance from the shock – at least within Cluster's 18.7×3.0 R_E orbit – is not an important bias for the distributions'shape.

As mentioned in the Introduction, the particle distribution features are essentially controlled by the solar wind speed and the shock geometry. Distribution (c) in Fig. 23.1 has $v_{sw} = 660$ km s^{-1}, and appears wider than other sampled distributions such as (a) or (b). However, the values of $\sigma_\parallel$ normalized to the solar wind speed are all in agreement with the 0.27–0.33 range of our previous finding [14]. Despite evident differences in the shape of these distributions, the FAB core distributions are remarkably well-fit by Maxwellians. We can anticipate that when tails are present the full-distribution standard deviation Σ will be larger than $\sigma_\parallel$ obtained from a

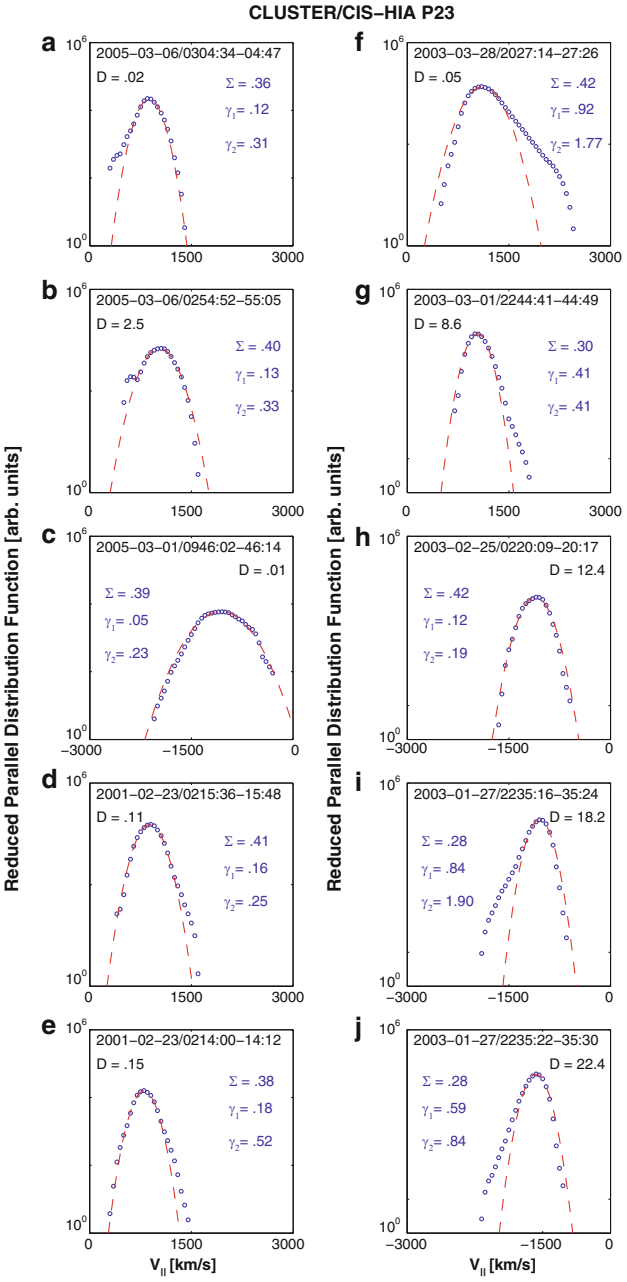

Fig. 23.1 Examples of reduced parallel distribution functions associated with FABs observed upstream of Earth's bow shock. In each frame, the *dashed line* represents the best Maxwellian fit. The observations are from the Cluster/CIS experiment

Maxwellian fit to the core. Moreover, all distributions appear asymmetric and it is common to see a low energy cut-off due to ions that could not overcome the shock speed; nevertheless, the low energy part of the distribution is satisfactorily fit by a Maxwellian. In order to quantify the distributions' asymmetry and 'squareness', we have calculated the skewness γ_1 and the kurtosis γ_2 of each distribution of Fig. 23.1; a numerical value of 3 has been subtracted from γ_2 values to make a null kurtosis for a standard normal distribution. The skewness in our case is a measure of the extent to which particles moving along one direction (in the beam frame) tend to have higher speeds than along the opposite direction. In plasma kinetic theory, the skewness is equivalent to the heat flux. The kurtosis is a measure of how peaked the function is, with values >0 indicating a narrow peak with wide tails (more 'extreme' values than a Gaussian distribution). The obtained values of the skewness γ_1 and the kurtosis γ_2 are indicated inside each panel of Fig. 23.1. As expected, the highest values of γ_1 are associated with distributions with strongest apparent tails. These determinations of the first moments of FAB reduced parallel velocity distribution functions lead to values of $\gamma_1 \sim 0.05$–0.92 and $\gamma_2 \sim 0.19$–1.69.

23.3 Accessible Source Regions and Velocity Filtering

With solar wind convection speeds an appreciable fraction of a backstreaming ion's parallel speed, it is important in a discussion of particle sources to distinguish between field lines and guiding center paths. Below we treat references to field lines as instantaneous mappings along field lines from one contact point to another, while guiding center references consider connections along particle paths that are affected by convection as well as particle parallel motions. Implicit in this is the idea that a particle originating at the shock on a field line threading a spacecraft cannot be observed unless the solar wind flow and the field are aligned, or the ion velocity is infinite. The size of the shock source region accessible to a spacecraft depends upon the direction of the magnetic field as well as the distance from the shock. Simple geometric considerations indicate that the source regions accessible to observers near the shock will be narrowest. The goal of this section is to provide an estimate of the time of flight effect in order to examine its possible impact on the shape of FAB ion distribution functions. For analytical simplicity we consider only the case of stationary upstream solar wind and IMF conditions. Here the bow shock is modeled as a paraboloid with nominal values for the sub-solar distance a_s and the flaring-parameter $b_s = 0.25/L$, where L is the semi-latus rectum. For zero pitch angle ions, the trajectory lies in the $\mathbf{Bv}_{sw}$-plane, which contains both the solar wind and the magnetic field directions. FAB ions that are detected by the spacecraft all emanate from the region where the $\mathbf{Bv}_{sw}$-plane intercepts the paraboloidal shock. Using simple algebra, the maximum length of the source region is obtained for a given spacecraft location, and solar wind flow and magnetic field directions. This region is bounded by the intercept of the field line threading the spacecraft ('A' in Fig. 23.2, described below) and the limiting ion guiding center trajectory, i.e., one that is tangent to the shock ('C').

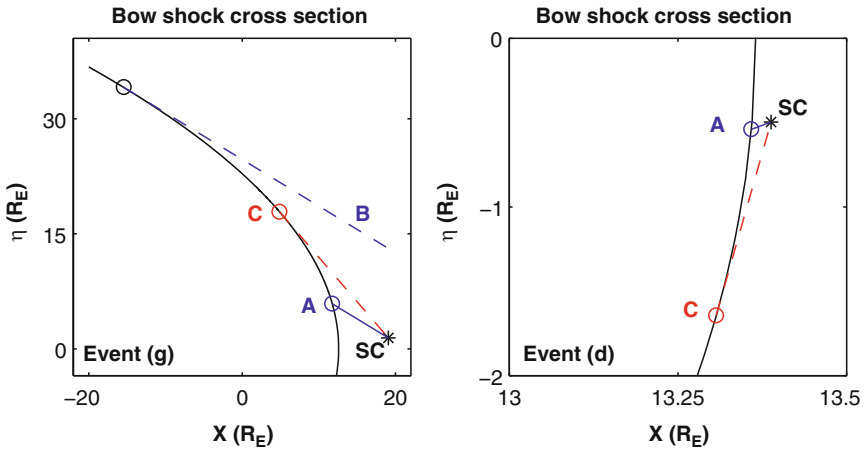

Fig. 23.2 Schematic diagram of the shock cross section in the $\mathbf{Bv}_{sw}$-plane showing the shock region source for events (d) and (g) of Fig. 23.1. The *dashed blue line* with label **B** indicates the IMF line tangent to the bow shock cross section. Only ions emanating between A and C can reach the spacecraft SC

Figure 23.2 illustrates the geometry for events (d) and (g) of Fig. 23.1. The curves shown do not represent the maximum extents of the paraboloidal bow shock, but instead the parabolic intersections of the $\mathbf{Bv}_{sw}$-plane with it. (The parameterizations of these intersection curves differ from those for the shock itself, and depend upon $\mathbf{B} \times \mathbf{v}_{sw}$ and the observer's location.) The X-axis represents the solar wind direction while the η-axis is an orthogonal direction in the $\mathbf{Bv}_{sw}$-plane. The dashed blue line 'B' shows the IMF field line in the $\mathbf{Bv}_{sw}$-plane that is tangent to the shock. For the paraboloidal model bow shock [4] we have adopted, distribution (d) is observed $D \sim 0.11\ R_E$ from the shock, while distribution (g) is observed at $D \sim 8.6\ R_E$. Distributions (d) and (g) have Gaussian cores and nearly identical normalized ion bulk speeds, with distribution (d) having a significantly larger standard deviation.

We can determine the variations $\Delta\theta_{AC}$ in the shock normal direction between points A and C. For event (g), with $D = 8.6\ R_E$, we find $\Delta\theta_{AC} = 25°$. This should lead to significant changes in parallel velocities at these differing source locations, according to a conventional quasi-adiabatic reflection picture, but velocity filtering must also be considered. Particles leaving point C with parallel speeds larger than the shock speed will travel further than $8.6\ R_E$ along the magnetic field direction in the time that it takes the field line to convect over to the spacecraft; velocity filtering in fact works to counter the increased beam speeds expected for increases in θ_{Bn} towards this extreme source location. In contrast, event (d) has $D = 0.11\ R_E$ and $\Delta\theta_{AC} = 2.6°$, and a locally-planar shock description should apply. Both distributions (d) and (g) were observed to have similar normalized peak beam speeds (2.5 and 2.6, respectively), suggesting similar nominal shock geometries. However, event (g) has a narrower normalized velocity spread ($\Sigma = 0.30$) than event (d) ($\Sigma = 0.41$); apparently, a larger $\Delta\theta_{AC}$ does not lead to a hotter parallel velocity

($v_\parallel$) distribution. Explanations of the thermal spread in $v_\parallel$ seem instead to require a process that is intrinsic to the shock, rather than this form of geometric argument. We note that the particular choice for the shock parameterization has little impact on the results. We found that the above $\Delta\theta_{AC}$ determinations, based on the parabolic bow shock model, are very similar to those obtained from an hyperbolic model [19] and an elliptical model [6].

A second consideration is the skewness and kurtosis for these distributions, which indicate the presence of a non-thermal tail. The tail for event (g) ($\gamma_1 = 0.41$, $\gamma_2 = 0.41$) is larger than that for event (d) ($\gamma_1 = 0.16$, $\gamma_2 = 0.25$), and is consistent with a larger spread in $\theta_{B\mathrm{n}}$ values for the contributing source regions. However, distribution (f), observed at a distance $D \sim 0.05\ R_\mathrm{E}$ from the nomimal shock, has even larger skewness and kurtosis values. This indicates that there is no a direct correspondance between the distance from the source region and the shape of the FAB distributions.

However, the thermal broadening intuitively expected for a larger range of $\theta_{B\mathrm{n}}$ values is not borne out for observed distributions considered here. The arguments above suggest that time of flight considerations are not of first importance in determining the shape of the FAB velocity distributions. Straightforward geometry shows that source point $\theta_{B\mathrm{n}}$ values will depend upon guiding center directions, and the span of these will depend upon distance from the shock and IMF direction. Although we should then expect a wider range of $v_\parallel$ values, and hence greater parallel temperatures, for a larger span of accessible source locations, the observed FABs in Fig. 23.1 do not support this (Σ is not correlated with $\Delta\theta_{AC}$). Likewise, if a broad range of source locations plays a role in producing non-thermal tails we should expect the skewness and kurtosis to increase with the observer's distance from the shock. This too is not observed. A possibility is that the particles arriving at the spacecraft may otherwise be constrained to source points near 'A' in Fig. 23.2. In that event, the observed thermal spread in $v_\parallel$ might instead be accounted for by localized effects at the shock. In the next section we present a geometric model employing fluctuations in the local shock normal direction to produce upstream velocity distributions with thermal features that are similar to those observed.

23.4 A Geometric Model

Two features in the observed upstream velocity distributions (Fig. 23.1) that we wish to explain are the thermal spreads that are greater than those for the incident solar wind beam [2] and the non-thermal tails [13] seen near oblique foreshock geometries. As outlined below, we produce these by assuming quasi-adiabatic reflection of incident solar wind ions in the presence of normally-distributed fluctuations in the local shock normal direction about some mean. A convolution of the resulting range of reflected parallel ion speeds leads to good qualitative agreement, even when making simplifying assumptions.

First, we re-derive expressions due to Paschmann et al. [17] in the plasma frame of reference. Reflection is assumed to conserve energy in the de Hoffman–Teller reference frame [5], with imperfect conservation of μ. Using primes to denote the de Hoffman–Teller frame, an incoming ion with a parallel velocity $v'_{i\parallel}$ is reflected with its parallel motion retaining a fraction δ of its incident momentum, $v'_{\parallel} = -\delta v'_{i\parallel}$, where $0 \leq \delta \leq 1$. The reflection is adiabatic for δ equal to unity. FAB observations indicate that δ is in the range 0.65–1.0 [3]. After transformation to the solar wind frame of reference (no primes), the pre- and post-encounter parallel velocities are related by $v_{\parallel} - V_{\rm s} = -\delta(v_{i\parallel} - V_{\rm s})$, where $V_{\rm s}$ is the shock speed introduced previously (Eq. 23.1). Since bulk solar wind ions are at rest, we obtain for the normalized parallel beam speed:

$$P = \frac{v_{\parallel}}{v_{\rm sw}} = -(1+\delta)\frac{\cos\theta_{V\rm n}}{\cos\theta_{B\rm n}} \tag{23.2}$$

In Eq. 23.2, the angles $\theta_{B\rm n}$ and $\theta_{V\rm n}$ are acute and obtuse, respectively, leading to a positive value for a backstreaming particles's parallel speed.

Equation 23.2 indicates that when the upstream flow $\mathbf{v}_{\rm sw}$ and magnetic field $\mathbf{B}$ are quasi-steady, the effects of shock geometry on normalized beam speed arise from variations in the normal orientation. Because the solar wind protons gyroradii are much smaller than the bow shock radius of curvature, we can reasonably apply an assumption of a locally planar shock for the interaction of individual thermal solar wind ions. However, the planar approximation is certainly not justified if small scale surface irregularities are present or when there is temporal variability. The development below presupposes that upstream ions emerge from a shock that has fluctuations in the local normal orientation. The model is equally applicable to temporal variability on times scales small compared to an ion distribution sampling time as it is to spatial variability on scales small compared with the (velocity filter) accessible source region. Here we regard $\mathbf{n}_0$ as the temporal (or regional) average of the local shock normal, which might be expected to agree well with normals obtained from quasi-empirical model shocks. Finally, we assume that the reflected particles escape upstream with speeds according to Eq. 23.2.

Let us now consider an escaping ion which propagates upstream of the shock where the normal direction makes an angle Φ with the respect to $\mathbf{n}_0$. We assume for this discussion that all variations of Φ are restricted to the $\mathbf{B}\mathbf{v}_{\rm sw}$-plane. This assumption has no physical basis, but we employ it to render the derivation tractable. In this 2D approximation, the shock normal direction is given by $\mathbf{n} = (\cos\Phi, \sin\Phi)$. Equation 23.2 can then be rewritten in terms of Φ:

$$P = -(1+\delta)\frac{\cos(\theta_{V\rm n0} - \Phi)}{\cos(\theta_{B\rm n0} - \Phi)} \tag{23.3}$$

with $\theta_{V\rm n0}$ and $\theta_{B\rm n0}$ angles characterizing the average local geometry based on $\mathbf{n}_0 = (1, 0)$.

Next we assume that the ions that reach the spacecraft leave the shock where the normal direction $\mathbf{n}$ is random while the average direction is $\mathbf{n}_0$. We have no a priori basis for expecting the effective shock normal to fluctuate uniformly about

its average, but assume a Gaussian distribution in Φ as an ansatz to be tested by observations. If we permit Φ to extend to $\pm\infty$, a naive application of Eq. 23.3 would include contributions for normal directions pointing into the shock. A rigorous treatment would truncate the range of Φ such that $-\pi/2 < \theta_{Bn0} - \Phi < \pi/2$, but for analytic simplicity we apply the simpler constraint $-\pi/2 < \Phi < \pi/2$. In practice FABs are observed for $45° \lesssim \theta_{Bn} \lesssim 75°$, and as we will show below, reasonable agreement with observations can be obtained for Gaussian variations in Φ with e-folding scales of just a few degrees. Consequently, only a tiny contribution in our analytic description will come from Φ variations that reverse the shock direction. With this in mind, we write the normalized probability density function of Φ as:

$$f_\Phi(\phi) = \frac{2}{\sigma_\Phi\sqrt{2\pi}} \frac{\exp^{-\frac{\phi^2}{2\sigma_\Phi^2}}}{\mathrm{erfc}(-\frac{\pi}{\sigma_\Phi\sqrt{2}}) - \mathrm{erfc}(\frac{\pi}{\sigma_\Phi\sqrt{2}})} \tag{23.4}$$

where σ_Φ is the standard deviation. Here we employ the convention used in probability theory, in which ϕ represents a particular value of the random variable Φ. Given the distribution $f_\Phi(\phi)$, and using Eq. 23.3, it is possible to derive the distribution $f_P(p)$ of escaping ion parallel velocities (normalized to the solar wind). The probability that the random variable P is equal or less than a value p is given by

$$\mathrm{Prob}(P \le p) = \int_0^p du f_P(u) \tag{23.5}$$

where $f_P(u)$ is the probability density distribution of P. The procedure for obtaining $f_P(p)$ can be found in any textbook on probability theory (see for example [1]); it is straightforward to show that:

$$\begin{aligned} f_P(p) = {} & \frac{2\Delta}{\sigma_\Phi\sqrt{2\pi}} \frac{|\sin(\theta_{Vn0} - \theta_{Bn0})|}{\mathrm{erfc}(-\frac{\pi}{\sigma_\Phi\sqrt{2}}) - \mathrm{erfc}(\frac{\pi}{\sigma_\Phi\sqrt{2}})} \\ & \times \frac{e^{-\left[\frac{1}{\sqrt{2}\sigma_\Phi}\tan^{-1}\left(\frac{p\cos\theta_{Bn0} - \Delta\cos\theta_{Vn0}}{p\sin\theta_{Bn0} - \Delta\sin\theta_{Vn0}}\right)\right]^2}}{\Delta^2 + p^2 - 2p\Delta\cos(\theta_{Vn0} - \theta_{Bn0})} \end{aligned} \tag{23.6}$$

where $\Delta = 1 + \delta$.

23.5 Results

For a perfectly adiabatic reflection ($\delta = 1$), the probability density function $f_P(p)$ is plotted for different values of σ_Φ as shown on Fig. 23.3. For $(\theta_{Vn0}, \theta_{Bn0}) = (160°, 48°)$, the maximum normalized beam speed is $P_0 = 2.81$. Both axes of Fig. 23.3 are scaled to allow a qualitative comparison with the observations shown in Fig. 23.1, with the y-axis spanning six orders of magnitude in space–phase

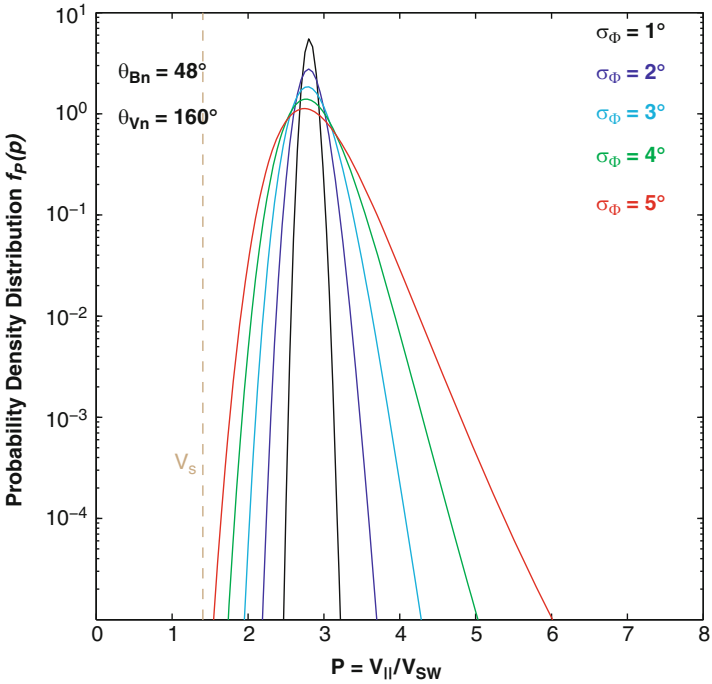

Fig. 23.3 Reduced parallel distribution functions obtained from Eq. 23.6 and a shock geometry corresponding to a normalized beam speed $P_0 = 2.81$. Each curve corresponds to a value of the standard deviation σ_Φ as indicated in the figure

density and the x-axis reaching ~3,000 km s^{-1}, for a typical solar wind speed of 375 km s^{-1}. The dashed vertical goldenrod line indicates the shock speed for (θ_{Vn0}, θ_{Bn0}) = (160°, 48°). Striking qualitative similarities between the observations and the results of the model illustrated in Fig. 23.3 are obvious. These include the high energy tails, and the Maxwellian form for the distributions just below the peak value. The tails harden for increasing values of σ_Φ, corresponding to increasing skewness values.

By taking moments of Eq. 23.6, we can quantify the shapes of the computed distributions and compare them with the observed distributions of Fig. 23.1. The panels in Fig. 23.4 show moments computed as functions of σ_Φ for adiabatic reflection ($\delta = 1$), with θ_{Vn0} fixed at 160°. Differently-colored symbols show the moments for three values of θ_{Bn0}: 45° (black), 50° (blue), and 55° (red). Panel (a) shows that escaping ion bulk speeds are independent of σ_Φ. However, there is a clear dependence upon σ_Φ for the 2nd, 3rd and 4th moments of $f_P(p)$. Of these higher moments, the second, Σ, shown in Panel (b), which can be related to the FAB parallel temperature, has the weakest σ_Φ-dependence. Most dramatic are the variations in γ_2, which indicate the presence of more-extreme values, corresponding to the high-energy tail. Similar trends are found for values of δ smaller than 1 (not shown); for these cases the dependence upon σ_Φ is weaker.

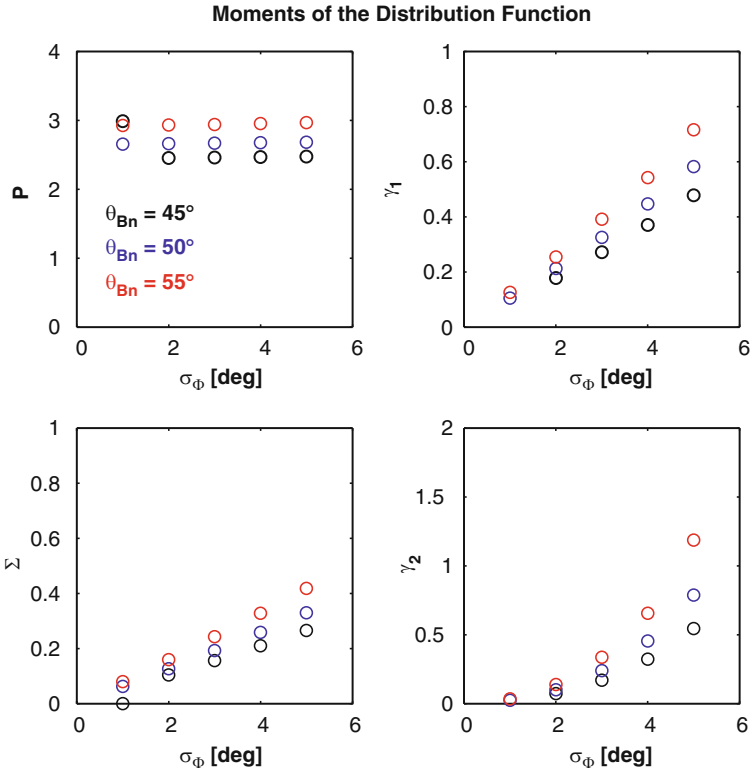

Fig. 23.4 First (P), second (Σ), third (*Skewness* γ_1) and forth (*Kurtosis* γ_2) order moments of the distribution $f_P(p)$ versus σ_Φ for three values of θ_{Bn0}

Finally we plot the dependence of the moments of Eq. 23.6 as a function of the normalized beam speed P, which we treat as a proxy for the shock geometry (cf. Eq. 23.1). Figure 23.5 shows the behavior of Σ and γ_1 for $\sigma_\Phi = 2°$ (black open circles), 3° (blue) and 4° (red). Both Σ and γ_1 show a nearly linear dependence upon P, with the slope steepening as σ_Φ increases. Reductions in δ to values lower than 1 do not produce significant changes.

23.6 Discussion

In this report we have attempted to explain the $v_\parallel$ profiles observed for upstream field-aligned beam distributions. The underlying model assumes quasi-adiabatic reflection from a shock having local normal orientations that fluctuate randomly about a mean value $\mathbf{n_0}$. Although the model assumes temporal changes in the shock normal direction at a specific point at the shock, the variations might also be viewed as resulting from spatial homogeneities at scales comparable to escaping ions gyroradii.

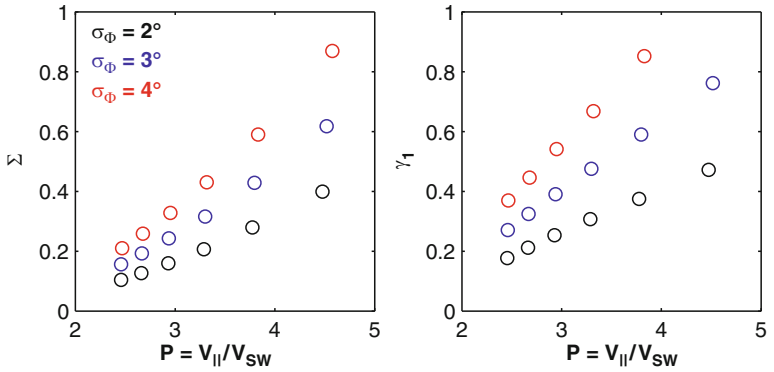

Fig. 23.5 Predicted second moment Σ and third moment γ_1 versus the beam speed P for three values of σ_Φ

Some support for both views is provided in the literature. For quasi-perpendicular geometries, moderate Alfvenic Mach number and low β-plasma, numerical simulations have shown that nonstationarity is inherent to the shock. During the shock reformation cycle, the shock structure including the foot, the ramp and the overshoot undergo spatio-temporal changes yielding significant local variations. Also, a relatively recent study from Cluster by [16] reported coherent 1,000–2,000 km wavelength oscillations in the foot and the ramp of the Earth's perpendicular bow shock. The authors interpreted the observations as ripples propagating across the shock surface along the magnetic field direction. It is obvious that the presence of such ripples would have a significant impact on the local geometry changes. A similar, but much slower, well-resolved variation of the local normal resulting from convection of large-amplitude ultra-low frequency (ULF) waves across the shock, and its consequences on backstreaming ions, was studied by Meziane et al. [12]. Another possibility is that small variations of the upstream plasma and field conditions, resulting from ubiquitous solar wind turbulence, would induce local changes in the shock normal as the shock adjusts to the variations according to well known conservation relations. Much of the ion foreshock is populated by magnetic pulsations, and it might seem that these could be a source of the normal orientation fluctuations. However, the larger pulsations tend to populate the quasi-parallel foreshock where FABs are not present, and would cause rather larger normal fluctuations than the few degrees required of our model. The model that we have developed is 2-dimensional, and unrealistically constrains the fluctuations of the source normal direction to the $\mathbf{Bv}_{sw}$-plane. We have no basis for expecting real fluctuations to have a preferred orientation, and such restrictions on degrees of freedom can be expected to exaggerate the influence of the variations. A complete treatment will necessarily require three dimensions. It is important to emphasize, as demonstrated in Sect. 23.2, that the shape of FABs is not an effect of the particle time of flight, although this might become an issue for beams observed sufficiently far from the source. No less important, the FABs presented in this report are not observed in association with ULF

waves, although they are considered to be the main free energy source for the latter. Absent such waves, we expect that FABs at moderate distances from the shock will suffer little diffusion, with their properties essentially unchanged.

Despite its limitations, our simple analytical model, based upon quasi-adiabatic reflection and normally distributed fluctuations in shock orientation, reproduces interesting features of FAB parallel velocity distributions. We have found that the range of predicted values of Σ are in remarkable agreement with the observations (Fig. 23.1), and require only modest angular fluctuation levels of $\sigma_\Phi = 2$–$4°$. Moreover, the qualitative features of this PDF are similar to those observed, and notably include high energy tails. The quantitative values for skewness γ_1 and kurtosis γ_2 can agree well with those obtained from the FABs of Fig. 23.1, although the agreement depends upon the value for θ_{Bn0}. The tails can be understood to result from the asymmetric influence of $1/\cos\theta_{Bn}$ in Eq. 23.2, which varies slowly for small values of θ_{Bn} and dramatically as $\theta_{Bn} \rightarrow 90°$. This effect is folded into the denominator of Eq. 23.6. Notably, the present model suggests that the tail has a local source, rather than originating in populations emanating from other regions of the shock. This result is in agreement with our previous finding regarding the source of the of the distribution tails [13]. Our model does not predict any kinks in the distribution, however.

It is important to note that the model predicts significant increases in the beam standard deviation and skewness when the shock geometry is increasingly perpendicular. This disagrees with the preliminary studies of Meziane et al. [13], who found that FAB tails are most apparent in oblique shock geometries, rather than perpendicular foreshocks. That work did not exhaustively isolate the roles of δ and θ_{Vn0}. Perhaps most significant, however, is the observational fact that foreshock wave activity can increase dramatically in oblique geometries. The sharp ULF wave boundary that is seen apparently separates field-aligned beams from gyrating ion beams and diffuse ions [14]. If, e.g., wave activity falls off exponentially upstream of this ULF boundary, a thus-far neglected fluctuation level might contribute to the non-thermal FAB tails, providing increases that follow the observational trends. This would suggest that the model might be improved by including a variable σ_Φ, which would increase with smaller values of θ_{Bn0}. Quantifying the actual variation would require a comprehensive study of observed upstream plasma and field fluctuations as θ_{Bn} and other parameters are varied.

Acknowledgements Work at U.N.B. is supported NSERC. Work at U.C. Berkeley is supported by NASA Grant NNG05GF99G. The authors are grateful to the International Space Science Institute for supporting topics related to shock acceleration.

References

1. Bertsekas, D.P., Tsitsiklis, J.N.: General Random Variables. Introduction to Probability. Athena Scientific, P. O. Box 805, Nashua, NH 03061-0805, USA (2002)
2. Bonifazi, C., Moreno, G.: Journal of Geophysical Research **86**, 4381 (1981)

3. Bonifazi, C., Moreno, G., Russell, C.T.: Journal of Geophysical Research **88**, 7853 (1983)
4. Cairns, I.H., Fairfield, D.H., Anderson, R.R., Carlton, V.E.H., Paularena, K.I., Lazarus, A.J.: Journal of Geophysical Research **100**, 47 (1995)
5. de Hoffman, F., Teller, E.: Physical Review **80**(4), 692 (1950)
6. Farris, M.H., Petrinec, S.M., Russell, C.T.: Geophysical Research Letters **18**, 1821 (1991)
7. Fuselier, S.A.: In: Engebretson, M., Takahashi, M., Scholer, M. (eds.) Solar Wind Sources of Magnetospheric Ultra-Low Frequency Waves, p. 91 (1994). American Geophysical Union
8. Hada, T., Onishi, M., Lembège, B., Savoini, P.: Journal of Geophysical Research **108**, 1233 (2003)
9. Kucharek, H., Möbius, E., Scholer, E., Mouikis, C., Kistler, L.M., Horbury, T., Balogh, A., Rème, H.: Annales Geophysicae **22**, 2301 (2004)
10. Lembège, P., Savoini, P.: Physics of Fluids B **4**, 3533 (1992)
11. Lobzin, V.V., Krasnoselskikh, V.V., Bosqued, J.M., Pinçon, J.L., Schwartz, S.J., Dunlop, M.: Geophysical Research Letters **34**, 05107 (2007)
12. Meziane, K., Wilber, M., Mazelle, C., LeQuéau, D., Kucharek, H., Lucek, E., Sauvaud, J.A., Hamza, A.M., Rème, H., Bosqued, J.M., Dandouras, I., Parks, G.K., McCarthy, M., Klecker, B., Korth, A., Bavassano-Cattaneo, M.B., Lundin, R.: Journal of Geophysical Research **109**, 05107 (2004). doi:10.1029/2003JA010374
13. Meziane, K., Wilber, M., Hamza, A.M., Mazelle, C., Parks, G.K., Rème, H., Lucek, E.: Journal of Geophysical Research **112**(A01101) (2007). doi:10.1029/2006JA011751
14. Meziane, K., Wilber, M., Hamza, A.M., Mazelle, C., Parks, G.K., Rème, H., Lucek, E.: Journal of Geophysical Research (2008).
15. Möbius, E., Kucharek, H., Mouikis, C., Georgescu, E., Kislter, L.M., Popecki, M.A., Scholer, J.M. M. Bosqued, Rème, H., Carlson, C.W., Klecker, A. B. Korth, Parks, G.K., Sauvaud, J.A., Balsiger, M.B. H. Bavassano-Cattaneo, Dandouras, I., DiLellis, L. A. M. Eliasson, Formissano, V., Horbury, W. T. Lennartsson, Lundin, R., McCarthy, M., P., M.J., Paschmann, G.: Annales Geophysicae **19**, 1411 (2001)
16. Moullard, O., Burgess, D., Horbury, T.S., Lucek, E.A.: Journal of Geophysical Research **111** (2006)
17. Paschmann, G., Sckopke, N., Asbridge, J.R., Bame, S.J., Gosling, J.T.: Journal of Geophysical Research **85**, 4689 (1980)
18. Scholer, M., Matsukiyo, S.: Annales Geophysicae **22**, 2345 (2004)
19. Slavin, J.H., Holzer, R.E.: Journal of Geophysical Research **86**, 11401 (1981)
20. Sonnerup, B. U. Ö.: Journal of Geophysical Research **74**, 1301 (1969)
21. Thomsen, M.F.: In: Stone, R.G., Tsurutani, B.T. (eds.) Collisionless Shocks in the Heliosphere: A Tutorial Review, p. 253 (1985). American Geophysical Union